



HAL
open science

Dynamic Energy Budget model suggests feeding constraints and physiological stress in black-lip pearl oysters, 5 years post mass-mortality event

Cristian Monaco, Nathanael Sangare, Gilles Le Moullac, Caline Basset, Corinne Belliard, Keiichi Mizuno, Diane L. Smith, Alain Lo-Yat

► To cite this version:

Cristian Monaco, Nathanael Sangare, Gilles Le Moullac, Caline Basset, Corinne Belliard, et al.. Dynamic Energy Budget model suggests feeding constraints and physiological stress in black-lip pearl oysters, 5 years post mass-mortality event. *Marine Pollution Bulletin*, 2021, 167, 112329 (9p.). 10.1016/j.marpolbul.2021.112329 . hal-04203435

HAL Id: hal-04203435

<https://hal.science/hal-04203435>

Submitted on 22 Jul 2024

HAL is a multi-disciplinary open access archive for the deposit and dissemination of scientific research documents, whether they are published or not. The documents may come from teaching and research institutions in France or abroad, or from public or private research centers.

L'archive ouverte pluridisciplinaire **HAL**, est destinée au dépôt et à la diffusion de documents scientifiques de niveau recherche, publiés ou non, émanant des établissements d'enseignement et de recherche français ou étrangers, des laboratoires publics ou privés.



Distributed under a Creative Commons Attribution - NonCommercial 4.0 International License

1 **Dynamic Energy Budget model suggests feeding constraints and physiological stress in black-lip**
2 **pearl oysters, 5 years post mass-mortality event**

3 Cristián J. Monaco^{a,*}, Nathanael Sangare^{a,b}, Gilles Le Moullac^a, Caline Basset^a, Corinne Belliard^a,
4 Keiichi Mizuno^a, Diane L. Smith^a & Alain Lo-Yat^a

5 ^a IFREMER, IRD, Institut Louis-Malardé, Univ Polynésie française, EIO, F-98719 Taravao, Tahiti,
6 French Polynesia

7 ^b UMR 9220 ENTROPIE, Institut de Recherche Pour le Développement, (IRD, Université de la
8 Réunion, Université de la Nouvelle-Calédonie, Ifremer, CNRS), B.P.A5, 98848, Nouméa, New
9 Caledonia

10 * Corresponding author: cristian.monaco@ifremer.fr

11

12 **ABSTRACT**

13 Mass-mortality events of marine species can disturb the structure of communities. While identifying
14 the causes of mass-mortality events is crucial for implementing recovery strategies, monitoring is
15 challenging in remote locations. Black-lip pearl oysters (*Pinctada margaritifera*) are farmed for
16 producing black pearls within remote atolls of French Polynesia. Previous mass-mortality events have
17 resulted in the collapse of oysters and other species; however, the causes and conditions that favour
18 recovery are unclear. We investigated the potential for oyster population recovery 5 years after a
19 mortality event at Takarua Atoll (Tuamotu Archipelago). Temperature, total chlorophyll-*a* (food),
20 growth and reproduction were monitored, and growth was simulated using a Dynamic Energy Budget
21 model. Despite favourable conditions, reduced growth and reproduction signalled an energetic deficit.
22 The model overpredicted growth, and supported the hypotheses that individuals are unable to profit
23 from the phytoplankton available and maintenance costs are high in Takarua, ultimately explaining
24 their poor physiological condition.

25

26 **Keywords:** Population collapse, population recovery, bivalve, aquaculture, tropical atoll, energetics

27

28 **1. Introduction**

29 Mass-mortality events of marine organisms have been increasingly documented across the world, due
30 to an intensification of both natural and anthropogenic-related stressors (Andréfouët et al., 2015;
31 Jackson, 2008; Sarà et al., 2021; Seuront et al., 2019). Should the affected species be important
32 ecological players and/or if they hold commercial or cultural value, the collapse of local populations
33 can have long-lasting negative consequences (Keenan et al., 2008). For resource managers and
34 producers, the strategies to manage the risk and impact of mass-mortality events include preventive
35 measures (e.g., considering the natural productivity of potential rearing sites), mitigative measures
36 (e.g., methods to reduce parasite load), and post-event measures (e.g., facilitating the recovery via
37 translocation campaigns) (McAfee et al., 2020; Nel et al., 1996; Nielsen and Petersen, 2019).

38 The population collapse of many important bivalve species due to overexploitation (e.g., rock
39 oysters globally; Beck et al., 2011) has recently led to major restoration efforts aiming to reattain
40 baseline population densities (McAfee et al., 2020). The success of these post-event measures
41 invariably depends on whether the *new* environmental conditions satisfy the requirements of the target
42 species. An alternative scenario emerges when the cause of the mass mortality is unknown, for
43 example, following microbial infections (Lallias et al., 2008; Samain and McCombie, 2008). In such
44 cases, because the culprit might effectively linger undetected in the system long after the event, the
45 success of restoration campaigns is often uncertain (McAfee et al., 2020). While a comprehensive
46 characterization of the bio-physical habitat can help gauge the suitability of the *new* habitat, the
47 practical constraints of examining every relevant variable, and the challenge of establishing cause-
48 effect relationships calls for complementary approaches. Individual-level indicators of physiological
49 condition, including both direct empirical observations and indirect model estimates of growth and
50 reproduction, can help assess the potential for recovery of populations after mass-mortality events
51 (Sawusdee et al., 2015).

52 The black-lip pearl oyster (*Pinctada margaritifera* Linnaeus 1758), which occurs naturally
53 across the tropical Indian and Pacific Oceans, supports the pearl-culture industry of French Polynesia
54 (Andréfouët et al., 2012). Farmers rely on the collection of wild oyster spats to produce pearls, but
55 because the activities are concentrated on a few atolls, most of which are located in the northern
56 Tuamotu Archipelago, the production of pearls is highly susceptible to environmental stochasticity of
57 natural and anthropogenic origin (Andréfouët et al., 2012). Since the onset of commercial pearl
58 farming in French Polynesia in the 1970s, two major mass-mortality events of *P. margaritifera*
59 populations have been documented in pearl-farming atolls: at Takapoto in 1985 and Takarua in 2014,
60 with profound knock-on effects on the livelihoods of producers and their families (Cabral, 1989;
61 Rodier et al., 2019). At Hikueru Atoll, where no pearl farming occurs, a wholesale community-level
62 mortality event was documented in 1994 (Adjeroud et al., 2001). Hypotheses to explain these events
63 include the detrimental effects of microalgae blooms and microbial infections (Cabral, 1989; Harris
64 and Fichez, 1995, Intes 1995) often associated with periods of reduced wind intensity and water
65 exchange between the lagoon and the open ocean (Andréfouët et al., 2015), but conclusive evidence is
66 unavailable. The historical recovery of a healthy stock of *P. margaritifera* at Takapoto within a period
67 of five years (G Haumani [agent of the *Direction des ressources marines*], *personal communication*)
68 suggests that the population might also recover functionally at Takarua.

69 Before the 2014 collapse, the wild population at Takarua was among the largest producers of
70 *P. margaritifera* spats and black pearls (Andréfouët et al., 2012). Although some pearl-farming
71 activity has been maintained after the mass-mortality event by translocating animals collected from
72 neighbouring atolls, the productivity has remained negligible compared to previous years. There is a
73 pressing need to determine the true potential for recovery of the wild stocks of the Takarua Atoll.
74 While no man-made strategies for population recovery have been implemented 5 years after the
75 population collapse, the introduction of mature individuals for pearl farming might effectively operate
76 as such, despite a male-biased sex ratio due to the species' protandric life cycle (Andréfouët et al.
77 2016; Thomas et al. 2016).

78 As a first approach for determining the potential for recovery of the Takaroa population of *P.*
79 *margaritifera*, we investigated the suitability of environmental conditions 5 years post mass-mortality
80 event, while explicitly considering the species' physiological requirements. Our analysis and data
81 included (1) *in situ* time series of seawater temperature and chlorophyll-*a* (Chl-*a*, proxy for food
82 availability), (2) measurements of individual growth and reproduction, and (3) energy budget
83 modelling based on the Dynamic Energy Budget (DEB) theory (Kooijman, 2010; Sangare et al. 2020;
84 Sousa et al., 2010). The empirical data (i.e., environmental and life-history traits) allowed direct
85 comparison of our observations against previous growth and reproduction data from neighbouring
86 atolls, while DEB modelling provided an indirect tool to examine physiological mechanisms
87 underlying the observed growth response. Assuming that the culprit of the mass-mortality event had
88 receded after 5 years, we expected that suitable environmental conditions would have yielded values
89 of growth and reproduction comparable to previous records from neighbouring atolls.

90

91 **2. Materials and methods**

92 *2.1. Sampling location and environmental conditions*

93 The Takaroa Atoll is part of the north-western Tuamotu Archipelago (French Polynesia). Our study
94 was done at the SCA QLES pearl-farm's concession, which is centrally located along the northeast-
95 southwest axis of the atoll, and skewed towards the wind-protected eastern boundary (14°27'34.4" S,
96 144°57'34.3" W). Takaroa is a semi-enclosed atoll with an area of 85 km², and average and maximum
97 depths of 26 and 47.5 m, respectively (Andréfouët et al., 2020) (Fig. 1).

98 Between January 30th and November 6th 2019, seawater temperature and total Chl-*a* were
99 recorded using a multiparameter sensor (NKE Smatch™) deployed at 5 m depth on a pearl-farm line.
100 Temperature and Chl-*a* data were averaged daily for the analyses. Because measurements of Chl-*a*
101 were subject to photoinhibition due to daylight (Charpy et al., 2012; Thomas et al., 2010), we only
102 used nocturnal measurements taken between 18:00 and 06:00. We excluded the Chl-*a* data between

103 17 and 26 April because the probe was covered with fouling agents. Linear interpolation was used to
104 fill this gap in data.

105 2.2. Empirical observations of growth and reproduction

106 We quantified the growth and reproductive potential of pearl oysters reared by a farmer in Takaroa
107 during 2019. Animals had been previously translocated to Takaroa as spats from the neighbouring
108 atoll of Takapoto (10 km south-west), and grown to an adult stage. Individuals were kept in standard
109 pearl-farming cages (Netlon™, 3-cm mesh size) attached to vertical ropes suspended ~5 m deep.
110 Cages were cleaned periodically to remove the biofouling. Animals used to examine growth were
111 marked with plastic tags and arranged in groups of 10 individuals per cage. Individuals used to assess
112 reproductive potential were sampled directly from the pearl-farm's stock (SCA QLES).

113 To quantify shell growth, we used 100 individuals measured on four dates (30/01/2019,
114 24/04/2019, 15/08/2019, and 06/11/2019), yielding three successive time intervals (interval 1, 84 d;
115 interval 2: 113 d; interval 3: 84 d). On each date, we measured the dorso-ventral length using callipers
116 (0.01-cm resolution). The initial shell length (mean \pm SD) was 8.84 ± 1.14 cm (range = 7.1 – 11.5
117 cm). The absolute growth rate (mm d^{-1}) was calculated as the difference in shell length between
118 successive measurements, divided by the number of days. The specific growth ($\% \text{d}^{-1}$) was calculated
119 by \log_{10} -transforming the two lengths, dividing by the number of days, and multiplying by 100
120 (Lugert et al., 2016). Note that growth was seemingly negative for several individuals, an artefact due
121 to the difficulty of successively measuring the shells along exactly the same axis. We were forced to
122 assume that this observation error was constant over time.

123 We examined the reproductive potential (gonad-development index) of animals collected
124 across six months (12/02/2019 – 23/07/2019), covering an important portion of the most active
125 reproductive period reported for *P. margaritifera* in French Polynesia (Fournier et al., 2012b). Thirty
126 individuals were collected weekly (total = 720 individuals), transported live to the laboratory
127 (IFREMER, *Centre du Pacifique*, Tahiti) and dissected. The gonado-visceral mass was fixed in 5%
128 saline formalin, rinsed after two days, and preserved in 70% ethanol for posterior analyses. Because

129 the gonads of pearl oysters are imbedded in the gonado-visceral mass, their contribution to the total
130 volume was estimated as the relative surface area of gonad tissues on a sagittal slide (Fournier et al.,
131 2012b; Moullac et al., 2013). We measured the surface area of gonads using images captured and
132 digitalized at 300 dpi with a scanner (Epson Perfection 4990 Photo) and processed using Adobe
133 Photoshop (CS3) and ImageJ (v.1.51j8). The shell length (mean \pm SD) of the animals used for
134 estimating gonad-development index was 9.36 ± 0.89 cm (range = 6.20 – 12.20 cm).

135 2.3. Dynamic Energy Budget (DEB) model growth predictions

136 Rooted in the robust Dynamic Energy Budget (DEB) theory, DEB models allow quantification of the
137 energy flow between the environment and an organism, and the dynamics of energy allocation
138 towards reserves, structure (i.e., growth), maintenance, maturation, and reproduction (Kooijman,
139 2010; Sousa et al., 2010). For a detailed perspective of the DEB model structure and assumptions see
140 Kooijman (2010) and Sousa et al. (2010). Here we highlight that DEB models can elegantly account
141 for both the influence of changes in food availability and body temperature on energy fluxes (e.g.,
142 Monaco et al., 2014; Monaco and McQuaid, 2018; Troost et al., 2010). We used the most recently-
143 parameterized DEB model for *P. margaritifera*, which was previously validated using populations
144 from the Tuamotu and Gambier Archipelagoes (Sangare et al., 2020, 2019), to predict changes in shell
145 length in response to the variability in seawater temperature and Chl-*a*. In this model, temperature
146 affects the rates at which energy is allocated among physiological functions (e.g., growth) following a
147 left-skewed thermal-performance curve (Fig. 2a). The parameter values that describe the curve were
148 estimated by Sangare et al. (2020), considering long-term responses by the species (Sangare et al.,
149 2020, 2019). The feeding process is described by a type-II functional response model, which predicts
150 relative ingestion as a function of food availability (Fig. 2b). The standard form of this curve depends
151 on the half-saturation coefficient parameter (X_K), which defines the food level that yields 50% of the
152 feeding capacity ($0.2 \mu\text{g Chl-}a \text{ L}^{-1}$ for *P. margaritifera*, Sangare et al., 2020). The model also includes
153 the somatic maintenance rate, $[\dot{p}M]$, a parameter that defines the volume-specific energy expenditure
154 of the individual ($5.4 \text{ J cm}^{-3} \text{ d}^{-1}$ for *P. margaritifera*, Sangare et al., 2020). Departures from the
155 species-specific $[\dot{p}M]$ values can indicate physiological stress (Pousse et al., 2019).

156 We used the DEB model, along with the daily measurements of temperature and Chl-*a* (see
157 2.1. *Sampling location and environmental conditions*), to predict the growth of each of the 100
158 individuals measured for the empirical growth determination (see 2.2. *Empirical observations of*
159 *growth and reproduction*). Because each animal was measured on four occasions, we examined the
160 growth over time in three successive intervals. We began the simulations assuming the initial size of
161 each animal at the beginning of each interval, while setting the reserves and reproduction state
162 variables at maximum and mean-observed levels, respectively (Monaco and McQuaid, 2018; Sangare
163 et al., 2020).

164 2.4. *Data analyses*

165 All data were analysed using R v3.6.2 (R Core Team, 2019).

166 We analysed the empirical growth data (shell length) for the 3 time intervals in two ways:
167 based on the absolute rate of change (i.e., mm d⁻¹), and based on the specific growth rate (i.e., % d⁻¹).
168 The former allowed comparing the observed values directly against those in the literature, while the
169 latter is a more robust estimate for comparing growth among individuals of different initial lengths
170 (Lugert et al., 2016). Animals were smaller than the asymptotic length reported for the species in
171 French Polynesia (~15-30 cm; Coeroli et al., 1984). To test for the effect of time interval on growth
172 rates and gonad-development index, we used the Kruskal-Wallis test (as data were non-parametric),
173 followed by a Dunn test for multiple comparisons.

174 To estimate the model fit we used the mean absolute error (*MAE*), computed as the mean
175 absolute difference between the empirical and predicted final shell lengths. We additionally tested the
176 hypotheses that modifying both the feeding functional response curve and the somatic maintenance
177 rate could further improve the model performance, and inform about unaccounted processes related to
178 feeding (e.g., Alunno-Bruscia et al., 2011; Thomas and Bacher, 2018) and/or physiological stress
179 (e.g., Pousse et al., 2019). Specifically, we ran 3 million additional simulations (100 individuals x 3
180 time intervals x 100 X_k values x 100 [*pM*] values) allowing the half-saturation coefficient parameter
181 (X_k) to vary between 0 and 5 (0.05-unit intervals) $\mu\text{g Chl-}a\text{ L}^{-1}$, and the volume-specific somatic

182 maintenance rate ($[pM]$) ranging between 0 and 20 (0.2-unit intervals) $\text{J cm}^{-3} \text{d}^{-1}$. The *best* values for
183 X_k and $[pM]$ were judged based on the lowest *MAE*.

184

185 **3. Results**

186 *3.1. Environmental variables*

187 We found differences in environmental drivers across the time intervals considered, particularly
188 regarding temperature dynamics (Fig. 3). Temperatures were highest and least variable during interval
189 1 (mean \pm SD = 30.1 ± 0.5 °C). As temperature decreased gradually during interval 2, the mean was
190 intermediate, but the variability was highest (mean \pm SD = 27.8 ± 1.1 °C). Interval 3 was in turn the
191 coolest, with intermediate variability (mean \pm SD = 27.3 ± 0.6 °C).

192 While the mean Chl-*a* was comparable across time intervals, the variability increased
193 progressively from interval 1 (mean \pm SD = 0.766 ± 0.195 $\mu\text{g Chl-}a \text{ L}^{-1}$) to interval 2 (mean \pm SD =
194 0.919 ± 0.468 $\mu\text{g Chl-}a \text{ L}^{-1}$) and interval 3 (mean \pm SD = 0.943 ± 0.767 $\mu\text{g Chl-}a \text{ L}^{-1}$) (Fig. 3).

195 *3.2. Empirical observations of growth and reproduction*

196 Time interval affected both estimates of empirical growth rate, absolute (Kruskal-Wallis test:
197 $df = 2$, $\chi^2 = 38.15$, $p < 0.001$) and specific ($df = 2$, $\chi^2 = 39.91$, $p < 0.001$) (Figs. 4a and 4b). Individuals
198 grew the fastest during interval 2, at intermediate level during interval 1, and the slowest during
199 interval 3 (Dunn test: specific growth, $p < 0.05$ for all contrasts) (Fig. 4a). The mean (\pm SD) absolute
200 shell growth was relatively low for the study location: 0.04 mm d^{-1} (± 0.05), 0.06 mm d^{-1} (± 0.05), and
201 0.01 mm d^{-1} (± 0.09) for intervals 1, 2, and 3, respectively (Fig. 4b). Mortality was negligible during
202 the growth-measurement period (only one of the 100 individuals died).

203 As growth, the gonad-development index was relatively low for the region, with an overall
204 mean (\pm SD) of 0.13 (± 0.11). Gonad-development index was higher during interval 1 (mean \pm SD =
205 0.20 ± 0.11) than 2 (mean \pm SD = 0.08 ± 0.07) (Kruskal-Wallis test: $df = 1$, $\chi^2 = 234.81$, $p < 0.001$)
206 (Fig. 4b), suggesting a spawning event at the population scale.

207 3.3. Dynamic Energy Budget (DEB) model growth predictions

208 Mean (\pm SD) predicted absolute growth was 0.21 mm d⁻¹ (\pm 0.02), 0.18 mm d⁻¹ (\pm 0.01), and 0.16 mm
209 d⁻¹ (\pm 0.01) for intervals 1, 2, and 3, respectively. Compared to the empirical growth data, the model
210 overpredicted the final shell length of oysters for intervals 1 (*MAE* = 1.46 cm), 2 (*MAE* = 1.42 cm),
211 and 3 (*MAE* = 1.34 cm) (Fig. 5). The overall *MAE* across intervals was 1.41 cm (Fig. 6).

212 Increasing the values of both the half-saturation coefficient parameter, X_{κ} , and the somatic-
213 maintenance rate, $[\dot{p}M]$, improved the overall model fit, reaching the lowest *MAE* (0.42 cm) with X_{κ} =
214 0.56 $\mu\text{g Chl-}a \text{ L}^{-1}$ and $[\dot{p}M]$ = 9.70 J cm⁻³ d⁻¹. At higher values of both parameters, the model fit was
215 relatively insensitive to changes in X_{κ} and $[\dot{p}M]$ (Fig. 6).

216

217 **4. Discussion**

218 We found that although temperature and total Chl-*a* in Takaroa appeared propitious for the
219 physiological performance of *P. margaritifera* in 2019, individuals grew remarkably slowly and
220 exhibited a relatively low reproductive effort, revealing an overall deteriorated energetic condition.
221 The DEB model simulations suggested that the underlying cause could be associated with both
222 individuals' inability to effectively consume the phytoplankton available in the water column, and
223 augmented physiological-stress levels. The finding that organisms continued to invest energy towards
224 reproduction supports the notion that energy allocation to growth and reproduction are not competing
225 processes in *P. margaritifera*, as previously demonstrated both empirically and theoretically (Sousa et
226 al., 2010). Ultimately, however, even if able to reproduce, the Takaroa population's recovery is
227 unlikely if individual growth is limited.

228 4.1. Environmental drivers

229 Temperature varied seasonally across the duration of the study, with a particularly warm brief
230 period (i.e., interval 1), and a protracted cooler period (intervals 2 and 3) (Fig. 3). The temperature
231 amplitude was within those reported previously for the same lagoon (min–max, 26.0–30.5 °C), and the

232 neighbouring atolls of Takapoto (min–max, 25.7–30.4 °C) and Manihi (min–max, 26.5–30.6 °C)
233 (Pouvreau and Prasil, 2001). Based on the thermal sensitivity of *P. margaritifera*, the thermal range at
234 which energy fluxes are maximised is ~28–32 °C (Fig. 2). Accordingly, the relative thermal
235 performance of individuals in Takarua was consistently close to the optimal for the duration of our
236 study. Short-term thermal acclimation experiments suggest that temperatures above 30 °C, as those we
237 recorded during two months, are detrimental to the growth of *P. margaritifera* (Le Moullac et al.,
238 2016). However, the thermal-sensitivity curve we used, which was fitted through the DEB parameter
239 estimation protocol, integrates thermal responses across the whole life cycle of the organism
240 (Kooijman, 2010; Sangare et al., 2020, 2019), and thus represents a more accurate measure
241 characterization of the animals' thermal performance across periods longer than one or two weeks.

242 The mean values of food availability (i.e., total Chl-*a*) at Takarua were stable across the 3
243 time intervals considered (Fig. 3), and considerably higher in 2019 than those reported previously for
244 other locations. At Takapoto, a study that compiled mean measurements from 1974 to 1998 reported
245 values ranging between 0.20 and 0.30 µg Chl-*a* L⁻¹ (Delesalle et al., 2001). At the lagoon of Ahe,
246 values from 2007 to 2010 ranged between 0.08 and 1.76 µg Chl-*a* L⁻¹ (Charpy et al., 2012; Fournier et
247 al., 2012b, 2012a; Thomas et al., 2010), and in 2013 between 0.30 and 0.80 µg Chl-*a* L⁻¹ (Pagano et
248 al., 2017). The temporal variability in our measurements, however, differed across time intervals (Fig.
249 3). The higher variability detected during intervals 2 and 3 reflects the recurrent presence of important
250 peaks in Chl-*a* values, which we did not observe in interval 1.

251 4.2. Empirical observations of growth and reproduction

252 Our empirical observations showed that animals could grow and reproduce throughout the duration of
253 the study (Fig. 4). Together with the observation that minimal mortalities were recorded during the
254 study, this might suggest that individuals maintained a positive energy balance, presumably pointing
255 to an auspicious population recovery (Sawusdee et al., 2015). However, relative to previous studies,
256 the observed growth rate was extremely low. Based on the von Bertalanffy growth model estimates
257 reported by Pouvreau and Prasil (2001) for the Takarua and Takapoto Atolls, the expected growth
258 rates of our animals were ~0.10 and ~0.09 mm d⁻¹, respectively, more than twice as fast as our

259 observations ($\sim 0.04 \text{ mm d}^{-1}$). *In situ* measurements at Takapoto (Coeroli et al., 1984) and Ahe
260 (Sangare et al., 2020) Atolls suggest growth rates $\sim 0.09 \text{ mm d}^{-1}$ for pearl oysters of similar size than
261 ours. Our growth rate observations were even lower than the estimated $\sim 0.08 \text{ mm d}^{-1}$ reported for the
262 lagoon of Vairao (Tahiti, French Polynesia), an area characterized by low primary production (Ky and
263 Le Moullac, 2017). These data revealed that, while individuals at Takarua had a positive scope for
264 growth, their energy budget was nevertheless strongly diminished.

265 The gonad-development index was lower (overall mean 0.13; Fig. 4b) than previously
266 reported. For the oligotrophic lagoon of Vairao (Tahiti), the mean value was 0.15, ranging between
267 0.05 and 0.23 (Lacoste et al., 2014). Additionally, at the more productive lagoon of Ahe, which
268 exhibits similar hydrobiological conditions to the Takarua Lagoon, the mean gonad-development
269 index was 0.17, ranging between 0.09 and 0.30 (Fournier et al., 2012b). The temporal variability in
270 the gonad-development index showed two distinct periods during our observations; high reproductive
271 potential before April and relatively low values thereafter. A similar trend was also documented by
272 Fournier et al. (2012b), who found higher values (0.22) between January and April, followed by a
273 period of lower gonad-development index (0.12) between April and July. This was attributed to a
274 strong and synchronous spawning event associated with a decrease in phytoplankton availability
275 (Fournier et al., 2012b). While we found no support for this relationship at Takarua, as mean Chl-*a*
276 did not change drastically across time intervals, the apparent spawning event we found between time
277 intervals 1 and 2 further supports the idea that despite the energetic constraints, individual
278 reproduction could be maintained.

279 The result that growth was relatively more affected than reproduction is particularly
280 interesting because it shows that these processes need not to compete for available energy resources,
281 as demonstrated empirically and theoretically for animals that exhibit indeterminate growth, including
282 invertebrates, fishes, reptiles, and amphibians (Heino and Kaitala, 1999; Kozłowski, 1996). But to
283 further understand why growth was more affected by the energy deficit than reproduction, it is
284 necessary to consider the process of energy allocation quantitatively. DEB formulations explicitly
285 remove the direct competition between these processes based on the κ -rule, where a fixed proportion

286 of mobilized reserves (κ) is directed to growth and somatic maintenance, and the rest ($1 - \kappa$) goes to
287 reproduction and maturity maintenance (Kooijman, 2010; Sousa et al., 2010). The costs of somatic
288 and maturity maintenance have priority over growth and reproduction, which is especially relevant if
289 the energy mobilized from reserves becomes limited (Monaco et al., 2014). Because somatic
290 maintenance is substantially costlier than maturity maintenance in *P. margaritifera* (Sangare et al.,
291 2020), its growth dynamics can be more sensitive to periods of reduced food availability than its
292 reproductive capabilities (Monaco et al., 2014). This scenario is consistent with the different
293 responses of growth and reproduction we found, and supports the notion that animals were indeed
294 nutritionally deprived.

295 4.3. Perspective from the Dynamic Energy Budget (DEB) model

296 The question of how to reconcile the seemingly abundant food availability (total Chl-*a*) at Takaroa
297 with the poor physiological condition in *P. margaritifera* individuals arises. A plausible explanation is
298 that the available food was not accessible by the organisms, for example, due to unmet requirements
299 of food particle size or nutritional quality (Dubois and Colombo, 2014; Ward and Shumway, 2004).
300 The DEB model simulations, using *in situ* measurements of total Chl-*a* and temperature as drivers,
301 allowed effectively testing this. By predicting faster growth than what was actually observed (Fig. 5),
302 the original model (Sangare et al., 2020) suggested either limitations to the organism's feeding (i.e.,
303 energy provisioning) or increased maintenance costs associated with physiological stress (i.e., energy
304 allocation). Minimizing the prediction error resulted in increases in the half-saturation coefficient by
305 1.8 fold and the somatic maintenance rate by 0.8 fold (Fig. 6), both being plausible explanations.
306 Because tropical lagoons are characteristically poor in nutrients, *P. margaritifera* exhibits a low half-
307 saturation coefficient that reflects its ability to profit from small increases in food, even at low
308 phytoplankton concentration (Pouvreau et al., 1999). The higher new estimate of the half-saturation
309 coefficient suggests a plastic response of the individual to adjust consumption of the microalgae
310 species available. The current model implementation, however, for simplicity assumes that food
311 availability is represented by total chlorophyll-*a*, and therefore cannot fully capture the complexities
312 of the feeding process in the wild (Dubois and Colombo, 2014; Sarà et al., 2003; Ward and Shumway,

313 2004). The finding that somatic maintenance cost was also higher than for the generalized *P.*
314 *margaritifera*, suggests the presence of an unknown stressor that reduced the physiological
315 performance of individuals in Takarua. For example, somatic maintenance can increase when bivalves
316 are exposed to low salinity or microalgae-related toxins (Lavaud et al., 2017; Pousse et al., 2019).

317 To improve the DEB model's ability to describe variability in the ingestion/assimilation of
318 food and somatic maintenance costs in *P. margaritifera*, further work is required in two axes: (1)
319 adequate characterization of the trophic (e.g., type, size, nutritional value of food items) and
320 physicochemical environment, and (2) restructuring the model to explicitly capture phenotypic
321 plasticity in the feeding and maintenance components (Sangare et al., 2020). Regarding feeding, the
322 literature, suggests that a likely culprit for the poor condition of *P. margaritifera* would be the
323 dominance of picophytoplankton (i.e., microalgae 0.2–2- μm cell size) in the water column, which is
324 too small for the organism to ingest (Loret et al., 2000; Pouvreau et al., 1999). Picophytoplankton
325 cells have been associated with previous mass-mortality events in the region (Cabral, 1989), and their
326 dominance over larger microalgae (i.e., nano and microphytoplankton) has increased over time in
327 Takapoto (Delesalle et al., 2001). Similarly, the quality of the diet of filter feeders also depends on the
328 inorganic content of the seston and the presence of non-chlorophyll-containing particles, some of
329 which could be digested (Ward and Shumway, 2004). Microplastics, another form of non-chlorophyll-
330 containing particles whose concentration is high in pearl-farming atolls, can in turn negatively affect
331 the physiological condition of pearl oysters (Gardon et al., 2018). It is also possible that regardless of
332 the food particle characteristics, the excess amount of food in Takarua (as suggested by high total Chl-
333 *a*) could have clogged the organism's cirri and labial palps, interfering with ingestion and assimilation
334 (Chávez-Villalba et al., 2013). Regarding the augmented somatic maintenance, two conceivable
335 drivers can be proposed for the Takarua Atoll: microplastics and toxic algae, both of which can
336 increase physiological stress (Gardon et al., 2018; Pousse et al., 2019).

337 Specific characteristics of the trophic and physicochemical environment can be
338 accommodated into DEB models. For instance, for benthic filter-feeder species whose ingestion of
339 carbon is dampened by the amount of inorganic matter in the water, the half-saturation coefficient is

340 calculated based on both organic and inorganic particles in the water (Thomas and Bacher, 2018;
341 Troost et al., 2010). Similarly, the dose-dependent toxic effects of microplastics or phytotoxins can be
342 computed on the basis of a variable somatic maintenance rate parameter (Pousse et al., 2019). Similar
343 developments could be implemented in the model of *P. margaritifera* to account for variation in food
344 type, including the presence of natural and exotic (e.g., microplastics; Gardon et al., 2018; Stamataki
345 et al., 2020) inorganic matter, and toxic compounds in tropical lagoons. Resolving these components
346 will improve the model's accuracy and broaden its scope (Sangare et al., 2020).

347 Finally, efforts that integrate the two working axes outlined above (i.e., characterizing the
348 trophic and physicochemical environment and improving the DEB model structure) are essential.
349 Comprehensive *in situ* descriptions of the environment is of course ideal. However, the remote nature
350 and difficulty in accessing many pearl-farming atolls call for practical approaches that can produce
351 data at high spatial and temporal resolution. While the rapid development of logging devices and
352 remote-sensing technologies is currently satisfying much of the demand for environmental data, their
353 estimates often depart significantly from the conditions truly experienced by the organism (Van
354 Wynsberge et al., 2017, 2020). Chl-*a* concentration estimates from fluorescent probes, for instance, do
355 not discriminate between the contribution of different phytoplankton groups, a development that
356 would likely help to greatly improve the DEB model predictions for *P. margaritifera*. Ultimately, the
357 accuracy and precision of this and other mechanistic models used across large and remote areas
358 depends on innovations to our *in situ* and possibly remote-sensing technologies (Canonica et al.,
359 2019).

360 4.4. Conclusion and future direction

361 Understanding the processes driving tropical marine mass-mortality events and the eventual recovery
362 of populations is particularly challenging when diagnostic data are difficult to produce, as is the case
363 for many Indo-pacific atolls and islands (Adjeroud et al., 2001; Cabral, 1989). Nevertheless,
364 understanding their underlying mechanisms is necessary to improve the management practices of
365 commercially-important and ecologically-relevant species, and to potentially prevent, or at least,
366 anticipate, similar episodes in the future.

367 Our study demonstrates that the physiological condition of *P. margaritifera* in the Takaroa
368 Atoll was suboptimal 5 years following a mass-mortality event, despite suitable temperatures and high
369 food availability in the years that followed. This was confirmed empirically by the relatively poor
370 growth and reproduction, and by DEB model simulations which overpredicted the final size of
371 animals raised in the lagoon. The apparent contradiction of having sufficient food but poor
372 performance indicated that the model deviation could be explained by an inadequate handling of the
373 feeding and physiological-stress processes by the predictive model. And finally, refitting the
374 functional response curve by modifying the half-saturation coefficient and the somatic maintenance
375 rate parameters demonstrated that a more nuanced formulation of these processes is needed for *P.*
376 *margaritifera*, if we are to accurately capture the physiological mechanisms underlying their slow
377 growth rate. By combining empirical evidence and the indirect inferences from DEB modelling, we
378 can formally propose the hypotheses that the currently unknown characteristics of the phytoplankton
379 community and physicochemical environment in Takaroa will delay the population's recovery.

380

381 **Acknowledgements**

382 This study was supported by the project Management of Atolls (MANA, ANR-16-CE32-0004). We
383 thank the *Direction des ressources marines* (DRM, French Polynesia) for support, and especially V
384 Liao for providing instruments and G Haumani for assisting during fieldwork. T Hauata (SCA QLES
385 pearl farm) assisted with the collection of animals and hosted the research team at Takaroa.

386 **5. References**

- 387 Adjeroūd, M., Andr fou t, S., Payri, C., 2001. Mass mortality of macrobenthic communities in the
388 lagoon of Hikueru atoll (French Polynesia). *Coral Reefs* 19, 287–291.
389 <https://doi.org/10.1007/PL00006962>
- 390 Alunno-Bruscia, M., Bourl s, Y., Maurer, D., Robert, S., Mazuri , J., Gangnery, A., Gouilletquer, P.,
391 Pouvreau, S., 2011. A single bio-energetics growth and reproduction model for the oyster
392 *Crassostrea gigas* in six Atlantic ecosystems. *Journal of Sea Research* 66, 340–348.
393 <https://doi.org/10.1016/j.seares.2011.07.008>
- 394 Andr fou t, S., Charpy, L., Lo-Yat, A., Lo, C., 2012. Recent research for pearl oyster aquaculture
395 management in French Polynesia. *Marine Pollution Bulletin* 65, 407–414.
396 <https://doi.org/10.1016/j.marpolbul.2012.06.021>
- 397 Andr fou t, S., Dutheil, C., Menkes, C.E., Bador, M., Lengaigne, M., 2015. Mass mortality events in
398 atoll lagoons: environmental control and increased future vulnerability. *Global Change*
399 *Biology* 21, 195–205. <https://doi.org/10.1111/gcb.12699>
- 400 Andr fou t, S., Thomas, Y., Dumas, F., Lo, C., 2016. Revisiting wild stocks of black lip oyster
401 *Pinctada margaritifera* in the Tuamotu Archipelago: The case of Ahe and Takaroa atolls and
402 implications for the cultured pearl industry. *Estuarine, Coastal and Shelf Science* 182, 243–
403 253. <https://doi.org/10.1016/j.ecss.2016.06.013>
- 404 Andr fou t, S., Genthon, P., Pelletier, B., Le Gendre, R., Friot, C., Smith, R., Liao, V., 2020. The
405 lagoon geomorphology of pearl farming atolls in the Central Pacific Ocean revisited using
406 detailed bathymetry data. *Marine Pollution Bulletin* 160, 111580.
407 <https://doi.org/10.1016/j.marpolbul.2020.111580>
- 408 Beck, M.W., Brumbaugh, R.D., Airolidi, L., Carranza, A., Coen, L.D., Crawford, C., Defeo, O.,
409 Edgar, G.J., Hancock, B., Kay, M.C., Lenihan, H.S., Luckenbach, M.W., Toropova, C.L.,
410 Zhang, G., Guo, X., 2011. Oyster Reefs at Risk and Recommendations for Conservation,
411 Restoration, and Management. *BioScience* 61, 107–116.
412 <https://doi.org/10.1525/bio.2011.61.2.5>

413 Cabral, P., 1989. Some aspects of the abnormal mortalities of the pearl oysters, *Pinctada*
414 *margaritifera* L. in the Tuamotu Archipelago. Aquacop IFREMER. Actes Colloq 9, 217–226.

415 Canonico, G., Buttigieg, P.L., Montes, E., Muller-Karger, F.E., Stepien, C., Wright, D., Benson, A.,
416 Helmuth, B., Costello, M., Sousa-Pinto, I., Saeedi, H., Newton, J., Appeltans, W., Bednaršek,
417 N., Bodrossy, L., Best, B.D., Brandt, A., Goodwin, K.D., Iken, K., Marques, A.C.,
418 Miloslavich, P., Ostrowski, M., Turner, W., Achterberg, E.P., Barry, T., Defeo, O., Bigatti,
419 G., Henry, L.-A., Ramiro-Sánchez, B., Durán, P., Morato, T., Roberts, J.M., García-Alegre,
420 A., Cuadrado, M.S., Murton, B., 2019. Global Observational Needs and Resources for Marine
421 Biodiversity. *Frontiers in Marine Science* 6, 367. <https://doi.org/10.3389/fmars.2019.00367>

422 Charpy, L., Rodier, M., Fournier, J., Langlade, M.-J., Gaertner-Mazouni, N., 2012. Physical and
423 chemical control of the phytoplankton of Ahe lagoon, French Polynesia. *Marine Pollution*
424 *Bulletin* 65, 471–477. <https://doi.org/10.1016/j.marpolbul.2011.12.026>

425 Chávez-Villalba, J., Soyez, C., Aurentz, H., Le Moullac, G., 2013. Physiological responses of female
426 and male black-lip pearl oysters (*Pinctada margaritifera*) to different temperatures and
427 concentrations of food. *Aquatic Living Resources* 26, 263–271.
428 <https://doi.org/10.1051/alr/2013059>

429 Coeroli, M., Gajllande, D.D., Landret, J.P., 1984. Recent innovations in cultivation of molluscs in
430 French Polynesia. *Aquaculture* 39, 45–67.

431 Delesalle, B., Sakka, A., Legendre, L., Pagès, J., Charpy, L., Loret, P., 2001. The phytoplankton of
432 Takapoto Atoll (Tuamotu Archipelago, French Polynesia): time and space variability of
433 biomass, primary production and composition over 24 years. *Aquat. Living Resour.* 8.

434 Dubois, S.F., Colombo, F., 2014. How picky can you be? Temporal variations in trophic niches of co-
435 occurring suspension-feeding species. *Food Webs* 1, 1–9.
436 <https://doi.org/10.1016/j.fooweb.2014.07.001>

437 Fournier, J., Dupuy, C., Bouvy, M., Couraudon-Réale, M., Charpy, L., Pouvreau, S., Le Moullac, G.,
438 Le Pennec, M., Cochard, J.-C., 2012a. Pearl oysters *Pinctada margaritifera* grazing on
439 natural plankton in Ahe atoll lagoon (Tuamotu archipelago, French Polynesia). *Marine*
440 *Pollution Bulletin* 65, 490–499.

441 Fournier, J., Levesque, E., Pouvreau, S., Pennec, M.L., Le Moullac, G., 2012b. Influence of plankton
442 concentration on gametogenesis and spawning of the black lip pearl oyster *Pinctada*
443 *margaritifera* in Ahe atoll lagoon (Tuamotu archipelago, French Polynesia). *Marine Pollution*
444 *Bulletin* 65, 463–470. <https://doi.org/10.1016/j.marpolbul.2012.03.027>

445 Harris, P., Fichez, R., 1995. Observations et mécanismes de la crise dystrophique de 1994 dans le
446 lagon de l'atoll d'Hikueru (Archipel des Tuamotu, Polynésie Française). ORSTOM, Notes et
447 Documents Oceanographie, Tahiti 45.

448 Gardon, T., Reisser, C., Soyez, C., Quillien, V., Le Moullac, G., 2018. Microplastics affect energy
449 balance and gametogenesis in the pearl oyster *Pinctada margaritifera*. *Environmental Science*
450 *& Technology* 52, 5277–5286. <https://doi.org/10.1021/acs.est.8b00168>

451 Heino, M., Kaitala, V., 1999. Evolution of resource allocation between growth and reproduction in
452 animals with indeterminate growth. *Journal of Evolutionary Biology* 12, 423–429.

453 Intes, A., 1995. The natural pearl shell populations in French Polynesia. *SPC Pearl Oyster Information*
454 *Bulletin* 8, 17–24.

455 Jackson, J.B.C., 2008. Ecological extinction and evolution in the brave new ocean. *Proceedings of the*
456 *National Academy of Sciences* 105, 11458–11465. <https://doi.org/10.1073/pnas.0802812105>

457 Keenan, E.E., Brainard, R.E., Basch, L.V., 2008. Historical and present status of the pearl oyster,
458 *Pinctada margaritifera*, in the Northwestern Hawaiian Islands, in: *Proceedings of the 11th*
459 *International Coral Reef Symposium*. Ft. Lauderdale, FL, USA, p. 12.

460 Kooijman, S.A.L.M., 2010. *Dynamic Energy Budget Theory for Metabolic Organization*, 3rd ed.

461 Kozłowski, J., 1996. Optimal allocation of resources explains interspecific life-history patterns in
462 animals with indeterminate growth. *Proc R Soc Lond B* 263, 559–566.

463 Ky, C.-L., Le Moullac, G., 2017. Shell growth performance of hatchery produced *Pinctada*
464 *margaritifera*: Family effect and relation with cultured pearl weight. *Journal of Aquaculture*
465 *Research and Development* 8. <https://doi.org/10.4172/2155-9546.1000480>

466 Lacoste, E., Le Moullac, G., Levy, P., Gueguen, Y., Gaertner-Mazouni, N., 2014. Biofouling
467 development and its effect on growth and reproduction of the farmed pearl oyster *Pinctada*
468 *margaritifera*. *Aquaculture* 434, 18–26.

469 Lallias, D., Arzul, I., Heurtebise, S., Ferrand, S., Chollet, B., Robert, M., Beaumont, A.R., Boudry, P.,
470 Morga, B., Lapègue, S., 2008. *Bonamia ostreae* -induced mortalities in one-year old
471 European flat oysters *Ostrea edulis*: experimental infection by cohabitation challenge. *Aquat.*
472 *Living Resour.* 21, 423–439. <https://doi.org/10.1051/alr:2008053>

473 Lavaud, R., La Peyre, M.K., Casas, S.M., Bacher, C., La Peyre, J.F., 2017. Integrating the effects of
474 salinity on the physiology of the eastern oyster, *Crassostrea virginica*, in the northern Gulf of
475 Mexico through a Dynamic Energy Budget model. *Ecological Modelling* 363, 221–233.
476 <https://doi.org/10.1016/j.ecolmodel.2017.09.003>

477 Le Moullac, G., Soyeux, C., Latchere, O., Vidal-Dupiol, J., Fremery, J., Saulnier, D., Lo Yat, A.,
478 Belliard, C., Mazouni-Gaertner, N., Gueguen, Y., 2016. *Pinctada margaritifera* responses to
479 temperature and pH: Acclimation capabilities and physiological limits. *Estuarine, Coastal and*
480 *Shelf Science* 182, 261–269. <https://doi.org/10.1016/j.ecss.2016.04.011>

481 Loret, P., Pastoureaud, A., Bacher, C., Delesalle, B., 2000. Phytoplankton composition and selective
482 feeding of the pearl oyster *Pinctada margaritifera* in the Takapoto lagoon (Tuamotu
483 Archipelago, French Polynesia): in situ study using optical microscopy and HPLC pigment
484 analysis. *Mar. Ecol. Prog. Ser.* 199, 55–67. <https://doi.org/10.3354/meps199055>

485 Lugert, V., Thaller, G., Tetens, J., Schulz, C., Krieter, J., 2016. A review on fish growth calculation:
486 multiple functions in fish production and their specific application. *Rev Aquacult* 8, 30–42.
487 <https://doi.org/10.1111/raq.12071>

488 McAfee, D., McLeod, I.M., Boström-Einarsson, L., Gillies, C.L., 2020. The value and opportunity of
489 restoring Australia’s lost rock oyster reefs. *Restor Ecol* 28, 304–314.
490 <https://doi.org/10.1111/rec.13125>

491 Monaco, C.J., McQuaid, C.D., 2018. Applicability of Dynamic Energy Budget (DEB) models across
492 steep environmental gradients. *Scientific Reports* 8, 16384. [https://doi.org/10.1038/s41598-](https://doi.org/10.1038/s41598-018-34786-w)
493 [018-34786-w](https://doi.org/10.1038/s41598-018-34786-w)

494 Monaco, C.J., Wetthey, D.S., Helmuth, B., 2014. A dynamic energy budget (DEB) model for the
495 keystone predator *Pisaster ochraceus*. *PLoS ONE* 9, e104658.
496 <https://doi.org/10.1371/journal.pone.0104658>

497 Moullac, G.L., Soyez, C., Sham-Koua, M., Levy, P., Moriceau, J., Vonau, V., Maihota, M., Cochard,
498 J.C., 2013. Feeding the pearl oyster *Pinctada margaritifera* during reproductive conditioning.
499 Aquaculture Research 44, 404–411. <https://doi.org/10.1111/j.1365-2109.2011.03045.x>

500 Nel, R., Cetzee, P., Van Niekerk, R., 1996. The evaluation of two treatments to reduce mud worm
501 (*Polydora hoplura* Claparède) infestation in commercially reared oysters (*Crassostrea gigas*
502 Thunberg). Aquaculture 141, 31–39.

503 Nielsen, P., Petersen, J.K., 2019. Flat oyster fishery management during a time with fluctuating
504 population size. Aquat. Living Resour. 32, 22. <https://doi.org/10.1051/alr/2019020>

505 Pousse, É., Flye-Sainte-Marie, J., Alunno-Bruscia, M., Hégaret, H., Rannou, É., Pecquerie, L.,
506 Marques, G.M., Thomas, Y., Castrec, J., Fabioux, C., Long, M., Lassudrie, M.,
507 Hermabessiere, L., Amzil, Z., Soudant, P., Jean, F., 2019. Modelling paralytic shellfish toxins
508 (PST) accumulation in *Crassostrea gigas* by using Dynamic Energy Budgets (DEB). Journal
509 of Sea Research 143, 152–164. <https://doi.org/10.1016/j.seares.2018.09.002>

510 Pouvreau, S., Jonquières, G., Buestel, D., 1999. Filtration by the pearl oyster, *Pinctada margaritifera*,
511 under conditions of low seston load and small particle size in a tropical lagoon habitat.
512 Aquaculture 176, 295–314. [https://doi.org/10.1016/S0044-8486\(99\)00102-7](https://doi.org/10.1016/S0044-8486(99)00102-7)

513 Pouvreau, S., Prasil, V., 2001. Growth of the black-lip pearl oyster, *Pinctada margaritifera*, at nine
514 culture sites of French Polynesia: synthesis of several sampling designs conducted between
515 1994 and 1999. Aquatic Living Resources 14, 155–163. [https://doi.org/10.1016/S0990-](https://doi.org/10.1016/S0990-7440(01)01120-2)
516 [7440\(01\)01120-2](https://doi.org/10.1016/S0990-7440(01)01120-2)

517 R Core Team, 2019. R: A language and environment for statistical computing. R Foundation for
518 Statistical Computing, Vienna, Austria.

519 Rodier, M., Longo, S., Henry, K., Ung, A., Lo-Yat, A., Darius, H., Viallon, J., Beker, B., Delesalle,
520 B., Chinain, M., 2019. Diversity and toxic potential of algal bloom-forming species from
521 Takaroa lagoon (Tuamotu, French Polynesia): a field and mesocosm study. Aquat. Microb.
522 Ecol. 83, 15–34. <https://doi.org/10.3354/ame01900>

523 Samain, J.F., McCombie, H. (Eds.), 2008. Summer mortality of Pacific oyster *Crassostrea gigas*: the
524 Morest project. Editions Quae.

525 Sangare, N., Lo-Yat, A., Le Moullac, G., Pecquerie, L., Thomas, Y., Beliaeff, B., Andréfouët, S.,
526 2019. Estimation of physical and physiological performances of blacklip pearl oyster larvae in
527 view of DEB modeling and recruitment assessment. *Journal of Experimental Marine Biology*
528 *and Ecology* 512, 42–50. <https://doi.org/10.1016/j.jembe.2018.12.008>

529 Sangare, N., Lo-Yat, A., Moullac, G.L., Pecquerie, L., Thomas, Y., Lefebvre, S., Gendre, R.L.,
530 Beliaeff, B., Andréfouët, S., 2020. Impact of environmental variability on *Pinctada*
531 *margaritifera* life-history traits: A full life cycle deb modeling approach. *Ecological*
532 *Modelling* 423, 109006. <https://doi.org/10.1016/j.ecolmodel.2020.109006>

533 Sarà, G., Giommi, C., Giacoletti, A., Conti, E., Mulder, C., Mangano, M.C., 2021. Multiple climate-
534 driven cascading ecosystem effects after the loss of a foundation species. *Science of The*
535 *Total Environment* 770, 144749. <https://doi.org/10.1016/j.scitotenv.2020.144749>

536 Sarà, G., Vizzini, S., Mazzola, A., 2003. Sources of carbon and dietary habits of new Lessepsian entry
537 *Brachidontes pharaonis* (Bivalvia, Mytilidae) in the western Mediterranean. *Marine Biology*
538 143, 713–722. <https://doi.org/10.1007/s00227-003-1118-4>

539 Sawusdee, A., Jensen, A.C., Collins, K.J., Hauton, C., 2015. Improvements in the physiological
540 performance of European flat oysters *Ostrea edulis* (Linnaeus, 1758) cultured on elevated reef
541 structures: Implications for oyster restoration. *Aquaculture* 444, 41–48.
542 <https://doi.org/10.1016/j.aquaculture.2015.03.022>

543 Seuront, L., Nicastro, K.R., Zardi, G.I., Goberville, E., 2019. Decreased thermal tolerance under
544 recurrent heat stress conditions explains summer mass mortality of the blue mussel *Mytilus*
545 *edulis*. *Sci Rep* 9, 17498. <https://doi.org/10.1038/s41598-019-53580-w>

546 Sousa, T., Domingos, T., Poggiale, J.-C., Kooijman, S.A.L.M., 2010. Dynamic energy budget theory
547 restores coherence in biology. *Phil. Trans. R. Soc. B* 365, 3413–3428.
548 <https://doi.org/10.1098/rstb.2010.0166>

549 Stamataki, N., Hatzonikolakis, Y., Tsiaras, K., Tsangaris, C., Petihakis, G., Sofianos, S.,
550 Triantafyllou, G., 2020. Modelling mussel (*Mytilus spp.*) microplastic accumulation. *Ocean*
551 *Sci.* 16, 927–949. <https://doi.org/10.5194/os-16-927-2020>

- 552 Thomas, Y., Bacher, C., 2018. Assessing the sensitivity of bivalve populations to global warming
553 using an individual-based modelling approach. *Global Change Biology* 24, 4581–4597.
554 <https://doi.org/10.1111/gcb.14402>
- 555 Thomas, Y., Garen, P., Courties, C., Charpy, L., 2010. Spatial and temporal variability of the pico-
556 and nanophytoplankton and bacterioplankton in a deep Polynesian atoll lagoon. *Aquat.*
557 *Microb. Ecol.* 59, 89–101. <https://doi.org/10.3354/ame01384>
- 558 Troost, T.A., Wijsman, J.W.M., Saraiva, S., Freitas, V., 2010. Modelling shellfish growth with
559 dynamic energy budget models: an application for cockles and mussels in the Oosterschelde
560 (southwest Netherlands). *Philosophical Transactions of the Royal Society B: Biological*
561 *Sciences* 365, 3567–3577. <https://doi.org/10.1098/rstb.2010.0074>
- 562 Van Wynsberge, S., Menkes, C., Le Gendre, R., Passfield, T., Andréfouët, S., 2017. Are Sea Surface
563 Temperature satellite measurements reliable proxies of lagoon temperature in the South
564 Pacific? *Estuarine, Coastal and Shelf Science* 199, 117–124.
565 <https://doi.org/10.1016/j.ecss.2017.09.033>
- 566 Van Wynsberge, S., Le Gendre, R., Sangare, N., Aucan, J., Menkes, C., Liao, V., Andréfouët, S.,
567 2020. Monitoring pearl farming lagoon temperature with global high resolution satellite-
568 derived products: An evaluation using Raroia Atoll, French Polynesia. *Marine Pollution*
569 *Bulletin* 160, 111576. <https://doi.org/10.1016/j.marpolbul.2020.111576>
- 570 Ward, E.J., Shumway, S.E., 2004. Separating the grain from the chaff: particle selection in
571 suspension- and deposit-feeding bivalves. *Journal of Experimental Marine Biology and*
572 *Ecology* 300, 83–130. <https://doi.org/10.1016/j.jembe.2004.03.002>

573 **Figure legends**

574 **Figure 1** Map of the Takaroa Atoll (Tuamotu Archipelago, French Polynesia), with our study location
575 indicated with a black point. The inset shows the position of the atoll within the Pacific Ocean.

576 **Figure 2** Dynamic Energy Budget model curves to describe the influence of (a) body temperature and
577 (b) total chlorophyll-*a* (proxy for food availability) on the rates of energy allocation of *Pinctada*
578 *margaritifera*. Parameter values that define the curves are from Sangare et al. (2020). Only the half-
579 saturation coefficient (X_{κ}) is indicated (by an arrow), as this is the only parameter we examined in this
580 study.

581 **Figure 3** Seawater temperature (°C) and total chlorophyll-*a* ($\mu\text{g Chl-}a \text{ L}^{-1}$) recorded in Takaroa during
582 three consecutive time intervals (interval 1, black, 30/01/2019 - 24/04/2019; interval 2, orange,
583 24/04/2019 - 15/08/2019; interval 3, light blue, 15/08/2019 - 06/11/2019). Panels (a) and (b) show
584 mean (\pm SD) daily values of temperature and chlorophyll-*a*, respectively. Panel (c) shows the overall
585 mean (\pm SD) temperature and total chlorophyll-*a* for each time interval.

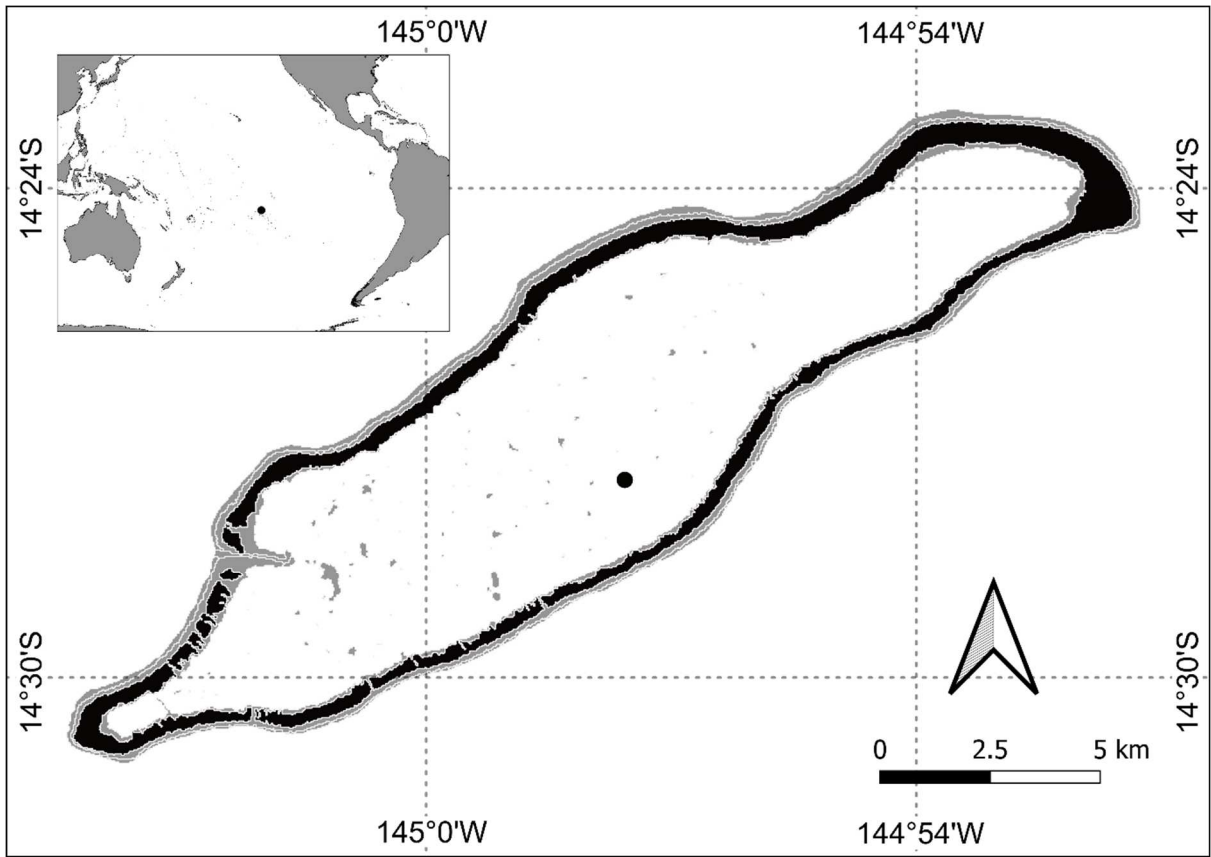
586 **Figure 4** Empirical growth and reproductive output of *Pinctada margaritifera* maintained in Takaroa.
587 (a) Specific and (b) absolute shell growth measured for 100 individuals during three consecutive time
588 intervals (interval 1, black, 30/01/2019 - 24/04/2019; interval 2, orange, 24/04/2019 - 15/08/2019;
589 interval 3, light blue, 15/08/2019 - 06/11/2019). (b) Gonado-somatic index measured weekly for 30
590 individuals between 12/02/2019 and 23/07/2019. Different letters above the boxplots indicate
591 significant differences between time intervals (Kruskal-Wallis test, Dunn test for multiple
592 comparisons, $\alpha = 0.05$). Boxes show the 25th and 75th percentiles, and horizontal lines the medians.
593 The whiskers illustrate the extreme values that are within 1.5 times the interquartile range. Points
594 represent outliers.

595 **Figure 5** Dynamic Energy Budget model predictions of growth (shell length, cm) for 100 *Pinctada*
596 *margaritifera* simulated for three consecutive time intervals (interval 1, black, 30/01/2019 -
597 24/04/2019; interval 2, orange, 24/04/2019 - 15/08/2019; interval 3, light blue, 15/08/2019 -
598 06/11/2019). The initial shell length for each individual was the ones of the animals used in the

599 empirical growth measurements. Lines illustrate model predictions. The box plots and points describe
600 the empirical measurements. The components of the box plots are as in Fig. 4.

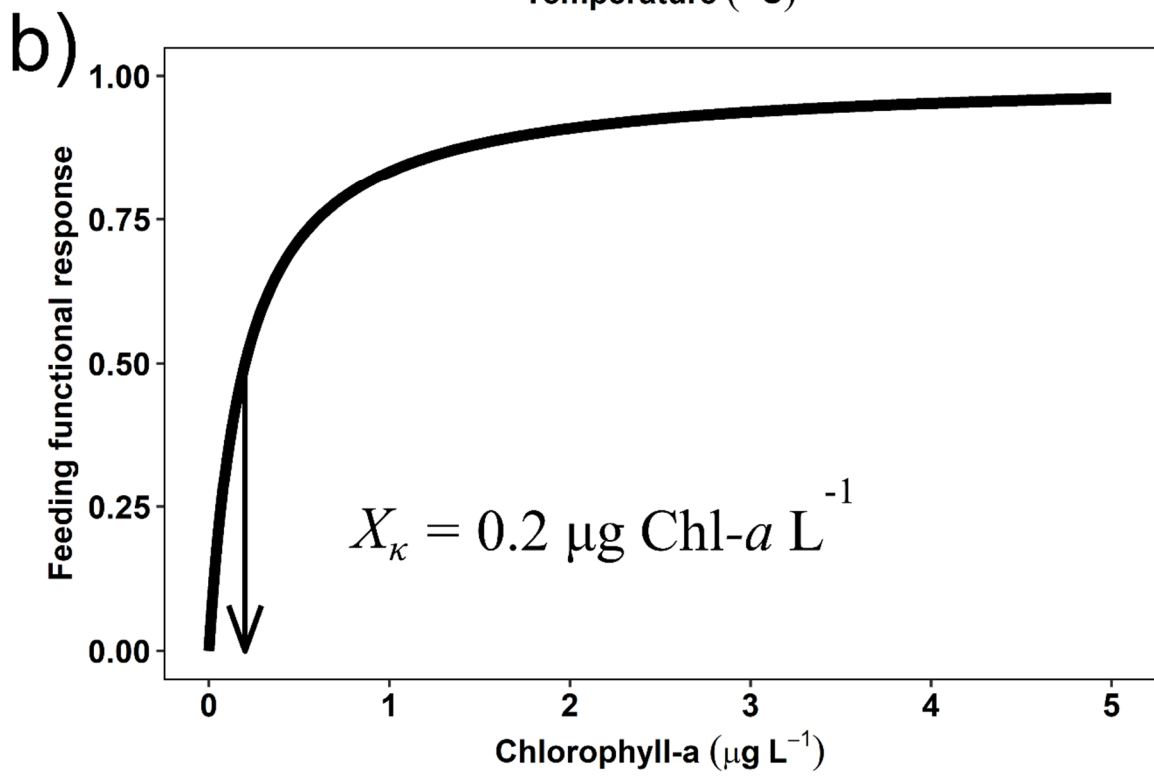
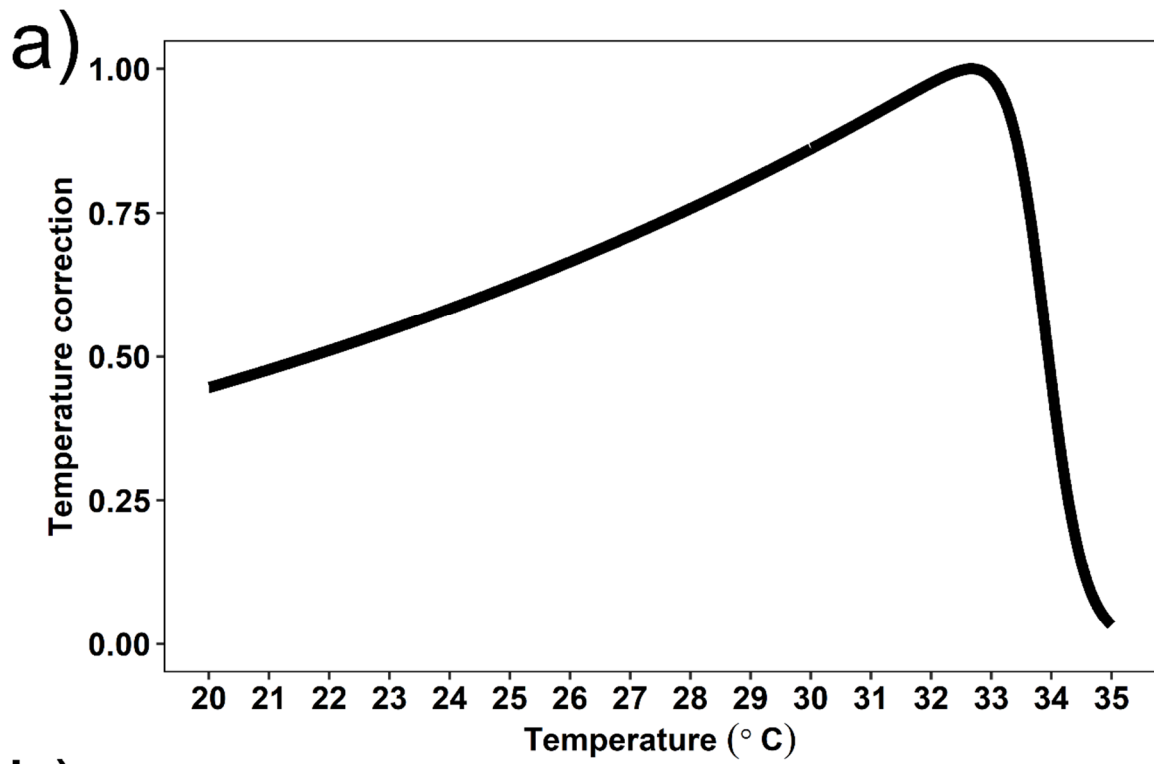
601 **Figure 6** Overall mean absolute errors (*MAEs*) for 10000 Dynamic Energy Budget (DEB) model
602 simulations of *Pinctada margaritifera* shell lengths. Each simulation was computed using a different
603 value for the parameters half-saturation coefficient (X_{κ} , $\mu\text{g Chl-}a\text{ L}^{-1}$), ranging between 0 and 5 (0.05-
604 unit intervals) $\mu\text{g Chl-}a\text{ L}^{-1}$, and the volume-specific somatic maintenance rate ($[\dot{p}M]$, $\text{J cm}^{-3}\text{ d}^{-1}$)
605 ranging between 0 and 20 (0.2-unit intervals) $\text{J cm}^{-3}\text{ d}^{-1}$. The circle indicates the X_{κ} and $[\dot{p}M]$
606 combination used in the original DEB model (Sangare et al., 2020), and the triangle indicates the
607 value that yields the lowest *MAE*. Cyan and red colours in the background represent low and high
608 *MAEs*, respectively. Blue contour lines separate *MAE* bins of 0.15-cm widths.

609 **Figure 1**



610

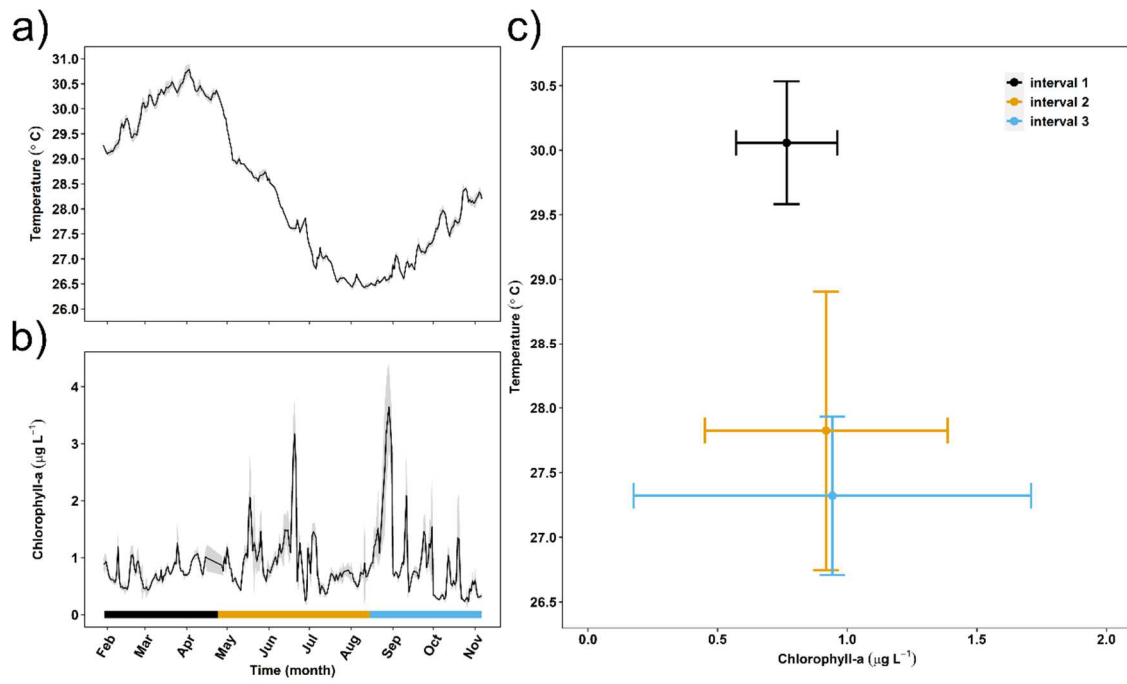
611 Figure 2



612

613

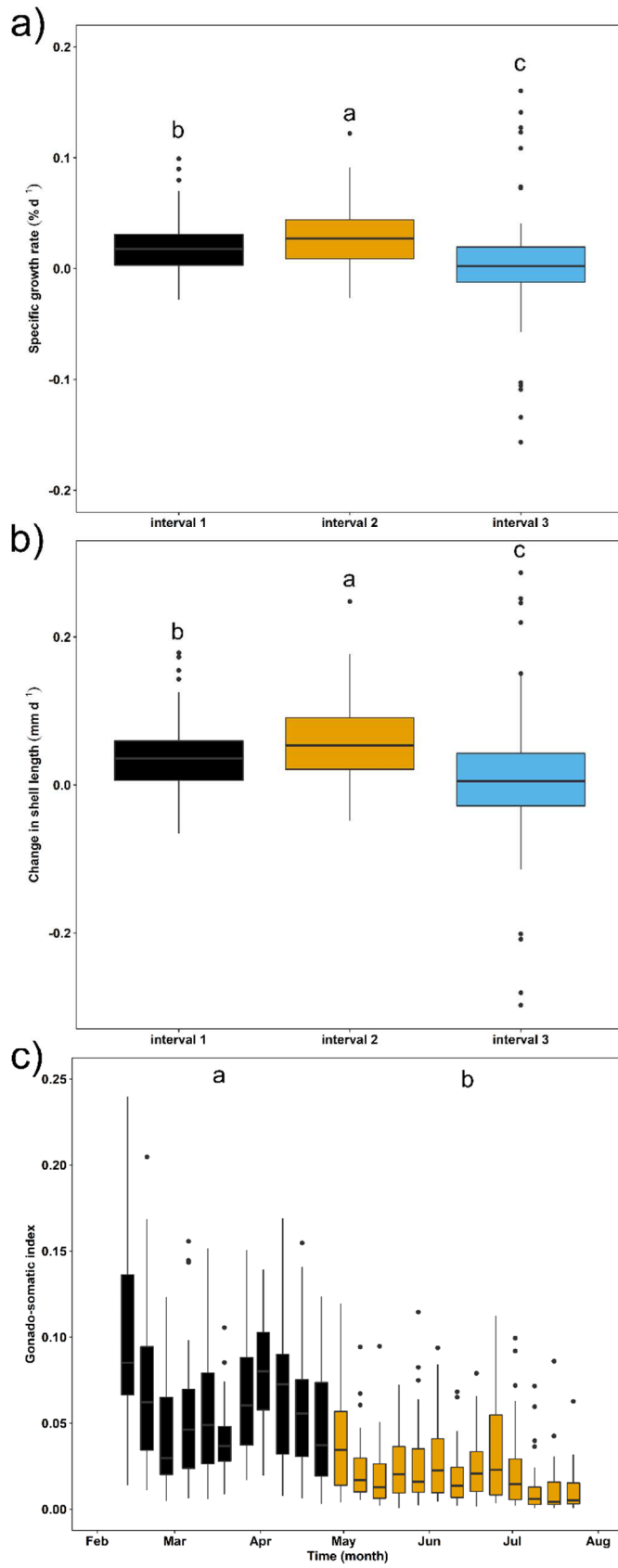
614 **Figure 3**



615

616

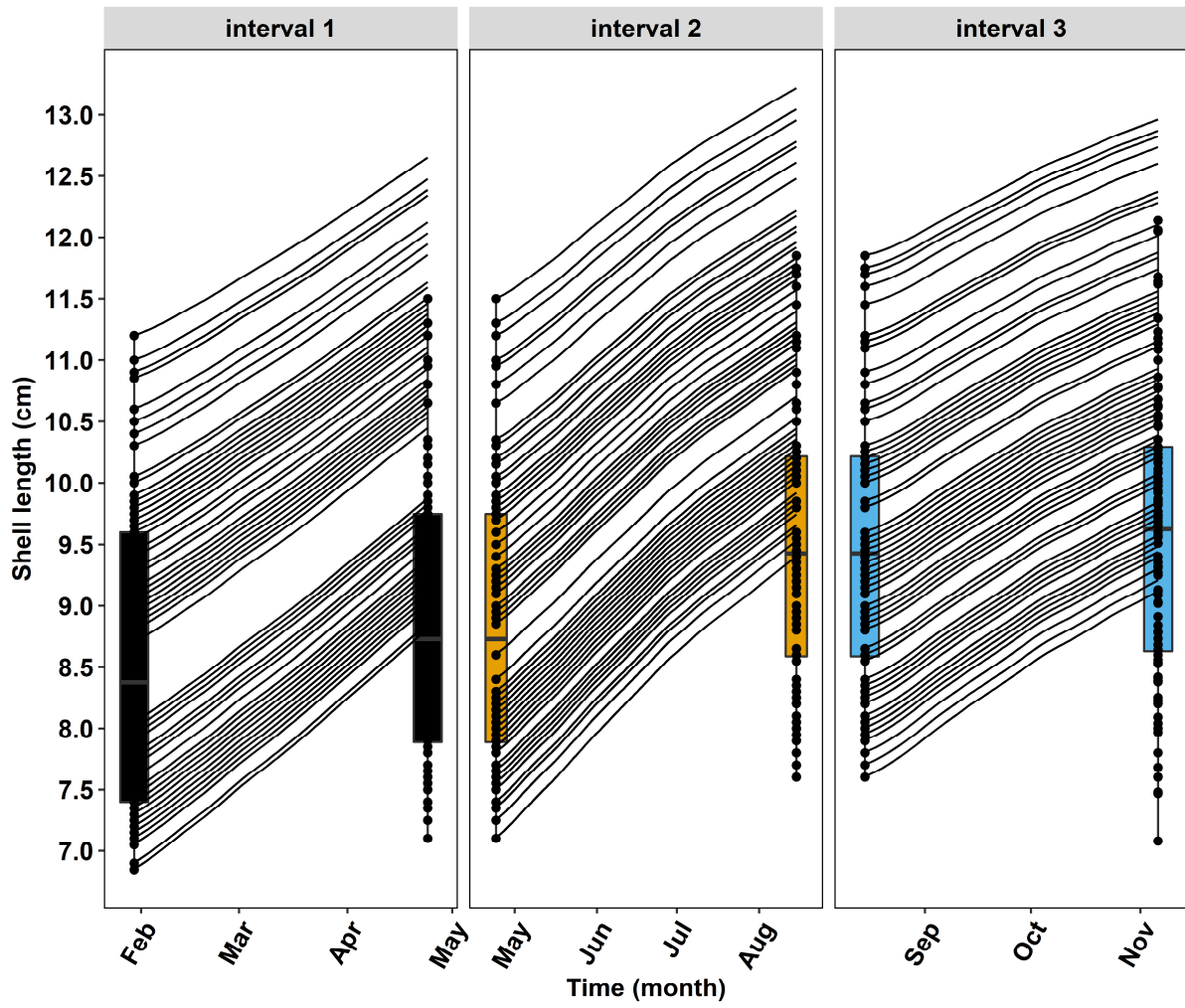
617 **Figure 4**



618

619

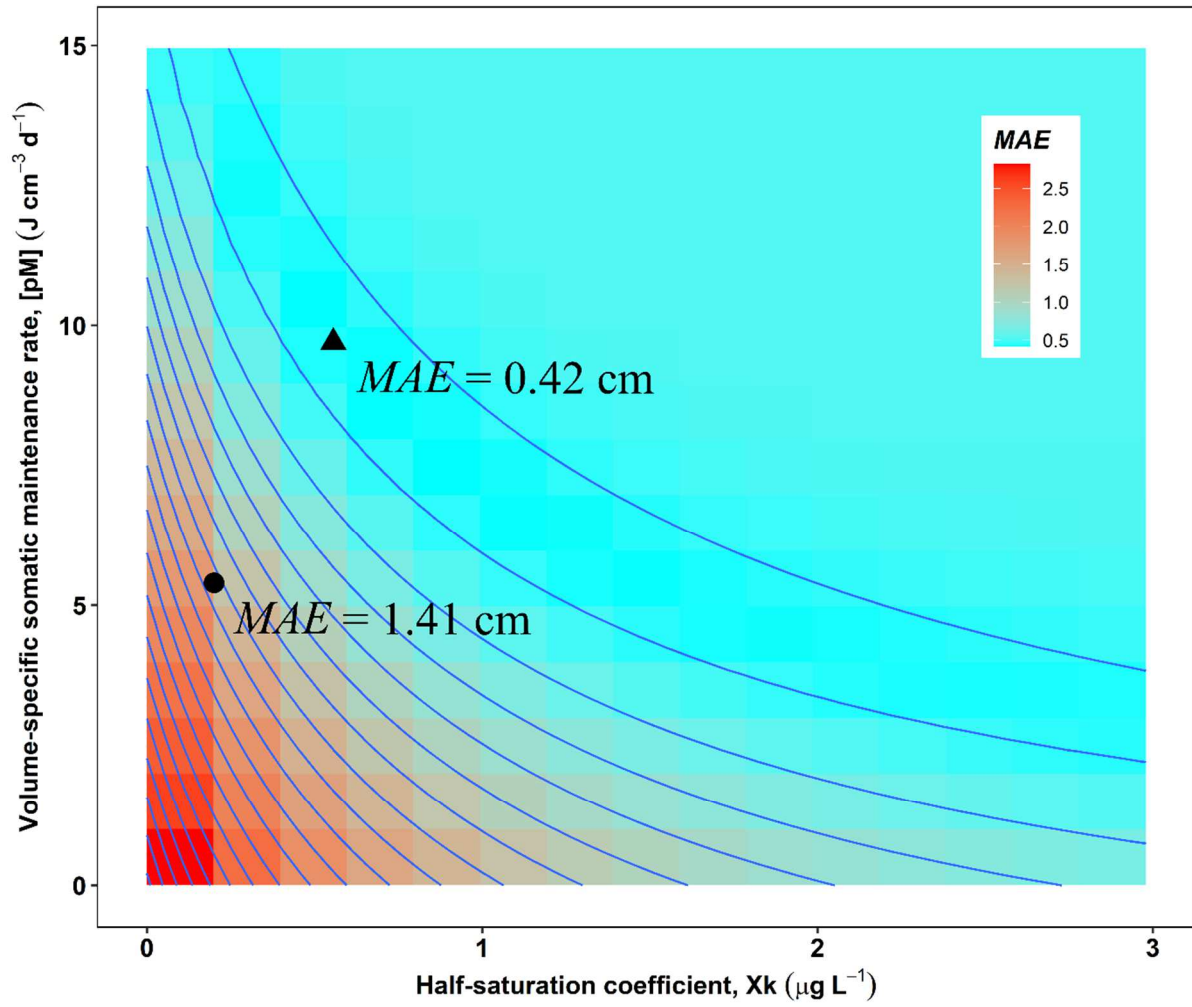
620 Figure 5



621

622

623 **Figure 6**



624